Geophysical Research Letters

RESEARCH LETTER
10.1029/2019GL083442

Jovian Injections Observed at High Latitude

D. K. Haggerty[1], B. H. Mauk[1], C. P. Paranicas[1], G. Clark[1], P. Kollmann[1], A. M. Rymer[1], G. R. Gladstone[2], T. K. Greathouse[2], S. J. Bolton[2], and S. M. Levin[3]

[1]The Johns Hopkins University Applied Physics Laboratory, Laurel, MD, USA, [2]Southwest Research Institute, San Antonio, TX, USA, [3]Jet Propulsion Laboratory, Pasadena, CA, USA

Abstract The polar orbit of Juno at Jupiter provides a unique opportunity to observe high-latitude energetic particle injections. We measure energy-dispersed impulsive injections of protons and electrons. Ion injection signatures are just as prevalent as electron signatures, contrary to previous equatorial observations. Included are previously unreported observations of high-energy banded structures believed to be remnants of much earlier injections, where the particles have had time to disperse around Jupiter. A model fit of the injections used to estimate timing fits the shape of the proton signatures better than it does the electron shapes, suggesting that electrons and protons are different in their abilities to escape the injection region. We present ultaviolet observations of Jupiter's aurora and discuss the relationship between auroral injection features and in situ injection events. We find, unexpectedly, that the presence of in situ particle injections does not necessarily result in auroral injection signatures.

Key Points:
- High-latitude observations at Jupiter reveal features of injections (L < 15 R_J) and associated auroral signatures not previously reported
- Included are a near equality of electron and ion injections, puzzling differences between their signatures and signatures of old injections
- There is no one-to-one correspondence between the in situ particle and auroral signatures of injections, contrary to literature expectations

Supporting Information:
- Supporting Information S1

Correspondence to:
D. K. Haggerty,
dennis.haggerty@jhuapl.edu

Citation:
Haggerty, D. K., Mauk, B. H., Paranicas, C. P., Clark, G., Kollmann, P., Rymer, A. M., et al. (2019). Jovian injections observed at high latitude. *Geophysical Research Letters*, *46*, 9397–9404. https://doi.org/10.1029/2019GL083442

Received 23 APR 2019
Accepted 5 AUG 2019
Accepted article online 9 AUG 2019
Published online 31 AUG 2019

1. Introduction

Energetic particle injections are frequently observed in planetary magnetospheres (Burch et al., 2005; Mauk et al., 1999, 2005; Paranicas et al., 2010). They comprise the particle signatures of the relatively sudden planetward displacements of particle populations within azimuthally constrained regions of space. At Jupiter and Saturn, it is thought that the continuous source of new cold plasma, originally from satellites close to the planet (Io and Enceladus, respectively), generates a circulation system whereby colder plasma must move outward and hotter plasmas (apparently energized within the middle magnetosphere) move inward, to conserve magnetic flux. Transient injections appear to be the agents for that transport. Particle injections also generate patch-like structures within the auroral emission regions (Dumont et al., 2014; Mauk et al., 2002).

A model from Mauk et al. (1999) describes key features of the injection phenomenon: (a) An azimuthally confined region of high phase space density is presumed to be radially injected within a specific meridian plane in a fashion that preserves the adiabatic invariants of the particles. (b) Given the general presence of a positive radial gradient in the phase space density at given values of the adiabatic invariants (e.g., Paranicas et al., 1990), a radial injection results in high intensity particles within the injection region adjacent to lower intensity particles on either side in the azimuthal direction. (c) These injected plasmas will rotate in an energy-dependent fashion because of the combined effects of rotational electric fields and magnetic gradient and curvature drifts. (d) Low energy particles will remain near the co-rotating injection site, but higher energy particles will magnetically drift away from that site. The protons will drift prograde while oppositely charged electrons will drift retrograde in the corotating frame. A spacecraft will tend to encounter particles associated with the injection in the following time order: the highest energy protons first, followed by lower energy protons, followed by very low energy electrons and ions, followed by low energy electrons, and lastly followed by the higher energy electrons.

In this letter we report new observations and findings of magnetospheric injections at Jupiter for particle energies >30 keV as revealed by the Juno spacecraft in a highly elliptical polar orbit (Bolton et al., 2017). The injected and dispersing particles extend into the very high magnetic latitude regions. As such, the Juno spacecraft can "track" an injection over a wide range of L shells where we can also infer the drift properties and make estimates about their lifetimes. We report on injection events observed during four periods in the northern hemisphere just prior to the spacecraft entering the auroral region. We also address the auroral manifestations of the injections enabled by the uniquely capable ultraviolet auroral imager on Juno.

This brief letter is intended to identify several new features of the injection phenomena overserved during several Juno orbits; future papers will provide a much more comprehensive examination of all of the Juno orbits

2. JEDI Observations

The Jupiter Energetic particle Detector Instrument (JEDI; see Mauk et al., 2013, for details) is an energetic ion mass (~30–20 MeV) and electron (~30–1,000 keV) spectrometer on Juno, designed to sample pitch angle distributions with magnetic field vectors provided by the magnetometer (Connerney et al., 2017). This report focuses on observations in the northern hemisphere prior to crossing the auroral region near perijove. Time periods are labeled with the closest perijove number (PJ#).

Figure 1 shows proton observations well above the magnetic equator prior for four consecutive perijoves. Each of these periods show various aspects of injection events, some contain long-lived structures with a peak in the energy spectrum (~400–800 keV), and others show shorter lived injections which exhibit energy dispersion. Heavy ion observations made simultaneously are difficult to characterize because of the poor heavy ion energy resolution (Supporting Information Figure S1).

Figure 1b (PJ8) shows the most dramatic series of injections. Here we see localized intensifications that are energy dispersed, with the higher energy protons arriving to the spacecraft prior to the arrival of the lower energy particles. These injections will be discussed in more detail later in this section.

Figure 1c (PJ9) shows a distinct older signature of proton injections lasting for hours (see overlaying white "+" signs used to guide the eye), an additional banded structure at higher energies, and hints of newer proton injections with little energy dispersion (see examples with black "^" signs). We identify the arching structure as the result of injection phenomena based on its similarity to features at Saturn (Paranicas et al., 2010). The peak intensity of the protons rises continuously in energy up to about 400 keV until about 16:00 UTC which corresponds to the minimum-L excursion of spacecraft. Had Juno penetrated to lower L values it would be our expectation that the peak energy would continue to rise. This characteristic is what Paranicas et al. (2010) found with older injections at Saturn, where at lower L values the injection signatures continue to rise in energy until they eventually dim to background rates.

Figure 1d (PJ10) shows a distinct long-lived proton injection feature peaking in energy near ~800 keV. Newer proton injections are observed prior to the older injection with little or modest energy dispersion. As compared with Figure 1c, there is a dramatic reduction of lower energy protons in the presence of the peak of the older injections, which creates what appears to be a void in the spectrogram at the lower energies. Because this region of space is filled with neutral gases from both Io and Europa (e.g., Smyth & Marconi, 2006), we speculate that charge exchange from neutral gases (favoring the loss of lower energies) had depleted these already-dim proton populations.

Figure 1a (PJ7) shows the weakest and most disordered injection signature covered in this study. Between 20:00 UT and ~22:30 UT we see a banded structure that may be one or more long-lived "older injections." Faint newer injections, some showing energy dispersion, are also observed within this region.

Figure 2 focuses on the PJ8 observations and the relationship with possible auroral injection signatures measured by the ultraviolet spectrometer (UVS) instrument on Juno (Gladstone et al., 2017). Here in addition to the proton spectrogram (same as in Figure 1b) we include electron spectrograms showing injections (Figure 2b) with an inverted energy scale. Many electron injections show energy dispersion with pronounced lower energy electrons followed by higher and higher energy electrons. A number of the electron injection features seem associated with proton injection features, as would be expected from the model described by Mauk et al. (1999). However, there does seem to be a modest time shift between proton and electron features at the position where the features meet at the lowest energies covered by JEDI (discussed in section 4.3). Two combined electron/ion injections are indicated as 1 and 2 that we quantitatively analyze in section 3. It is significant that ion injections are just as visible, distinct, and numerous as are the electron injections, contrary to measurements reported close to the equator (Mauk et al., 1999).

The UVS false-color image is of the northern ultraviolet aurora. UVS is described by Gladstone et al. (2017), and analysis of UVS images is presented by Bonfond et al. (2017). The different colors correspond to different

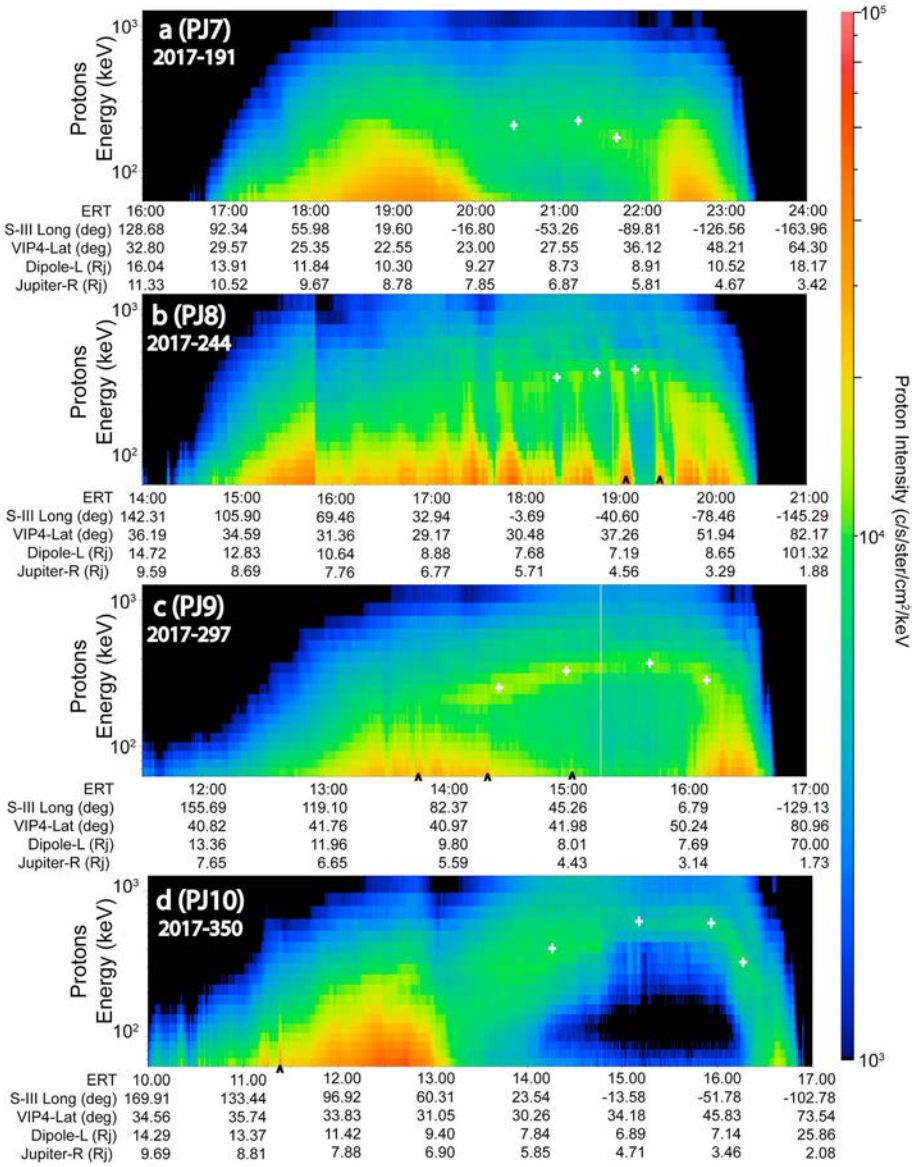

Figure 1. Proton energy-time spectrograms (Panels a–d) for four different Juno high-latitude, near perijove (PJ) periods. The Panel b discontinuity near 1550 is an instrument mode change. The abscissas we show the Universal time, system-III longitude, magnetic latitude, and dipole L derived from the VIP-4 model (Connerney et al., 1998), Jovian radial distance (R).

UVS spectral bands, which are interpreted (see also Gérard et al., 2014) as corresponding to different energies for the electrons striking the atmosphere, with red corresponding to high energies, green to intermediate energies, and blue to lower energies; white indicates a mix of energies. Such colorations are thought to be sensitive to electron energies ranging from 50 to 500 keV (Gérard et al., 2014). Overlaying this "context" map, comprised of 80 swaths of the UVS slit across the northern auroral region during 2036-2116 UTC (i.e., just after the JEDI data of A and B were acquired), is the magnetic footprint of the Juno spacecraft trajectory calculated using the JRM09 internal magnetic field model (Connerney et al., 2018) combined with a magnetodisc model (Connerney et al., 1981) describing the external field. The time over which the image was accumulated corresponds to the thickened portion of the projected Juno trajectory (after 20:36 UT).

This UVS map shows a number of isolated patch-like regions (most clearly to the upper right of the main aurora and called snow cones by the team) that are identified as being associated with magnetospheric

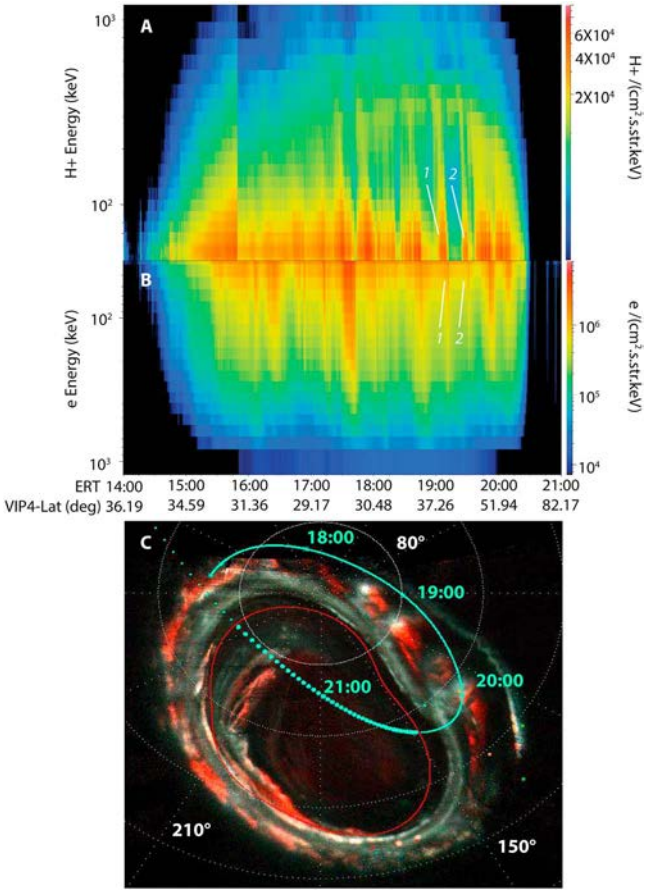

Figure 2. Proton and electron energy-time spectrograms (Panels a andb) for the near PJ8 time period (same time as Panel b in Figure 1), and an auroral image (Panel c) taken during a similar time period. Two injections (labeled 1 and 2) are highlighted for detailed analysis. The UVS false-color map of Jupiter's northern aurora (Panel c) was observed from 20:26 through 21:16 UTC. See the text for a discussion of the meanings of the different colors and details about the magnetically mapped position of the Juno spacecraft (blue line). The discontinuity in Panel a near 15:50 corresponds to an instrument mode change.

injections on the basis of previous work (Dumont et al., 2014; Mauk et al., 2002). Previous observations from Hubble Space Telescope show that the injection patches evolve slowly and corotate with Jupiter over hour time scales (Dumont et al., 2014, 2018; Mauk et al., 2002). A striking aspect of these features, is the dispersion in color that is seen within each patch. What we see within the injection-induced patches is that the lower energies (white portion) lead, and the higher energies (red portion) lag, the rotational motion of the auroral features (rotating counter clockwise on the figure), as also reported by Dumont et al. (2018) using Hubble Space Telescope multispectral imaging. Because much more work is needed to quantify the energies associated with the different colors, we can only say at the point in time that the patches are at least several hour old.

It is interesting that the specific locations of these energy dispersive injection emissions do not all fall directly along the track of the spacecraft. At 20:00 UTC we see injections both in situ (Figures 2a and 2b) and within the auroral image (Figure 2c) roughly along the same magnetic field line. However, while we see particle injection features at Juno near 19:00 (Figures 2a and 2b), we see no obvious auroral injection signatures at 19:00 along the Juno ground track, contrary to the single good correspondence reported by Mauk et al. (2002). Errors in magnetic mapping using the JM09 model are expected to be much less than 1° based on the field model's success in matching the observed auroral spots for the Jovian moons (John E. P. Connerney, private communication, 28 July 2019). Also, while the Juno trajectory position at 19:00 was not imaged until a couple of hours later, because auroral patches corotate and stay roughly where they are over hour time frames (Dumont et al., 2014, 2018; Mauk et al., 2002), signatures of the JEDI-observed injections should be visible in the images if the JEDI-observed injections were resulting in electron precipitation at the time the auroral image was taken. It is clear from this well-sampled region that injections observed in situ do not yield a one-to-one correspondence with auroral images. The auroral injection features observed at similar longitudes map to L positions that are outside of Juno's position. We address the discrepancies in section 4.2.

3. Modeling In Situ Injections

One may model the particle injections based on the Mauk et al. (1999) scenario described in section 1. The specifics of that model for Juno are provided in Appendix A.

Two specific discreet injections (indicated in Figure 2) are modeled here. The specific events chosen for this analysis were fairly isolated from other injections and had the best qualitative (visual inspection) time correlation. We looked at each JEDI energy channel which contained the associated dispersive particles and fit a Gaussian to the intensity time series data to find the centroid and standard deviation of the dispersion in each given energy channel. We captured that information along with the channel energies, and the spacecraft L and magnetic latitude positions and analyzed that information in the fashion described in Appendix A. Figure 3 shows the results where the red dots represent the observations for the electrons and the blue dots for the protons. The solid lines corresponding to each set of dots represent the model fit to the observations. While we have analyzed these injections in a number of different ways, for Figure 3 we have here optimized the fit strictly using the protons and then just laid the corresponding electron model onto the plot to see how well that procedure yields a good fit for the electrons. For Events 1 and 2 it appears that the protons (from the lowest through the highest energies) are well fit with our chosen model, while the shapes of the electron dispersion curve show significant deviations from the shape dictated by the model.

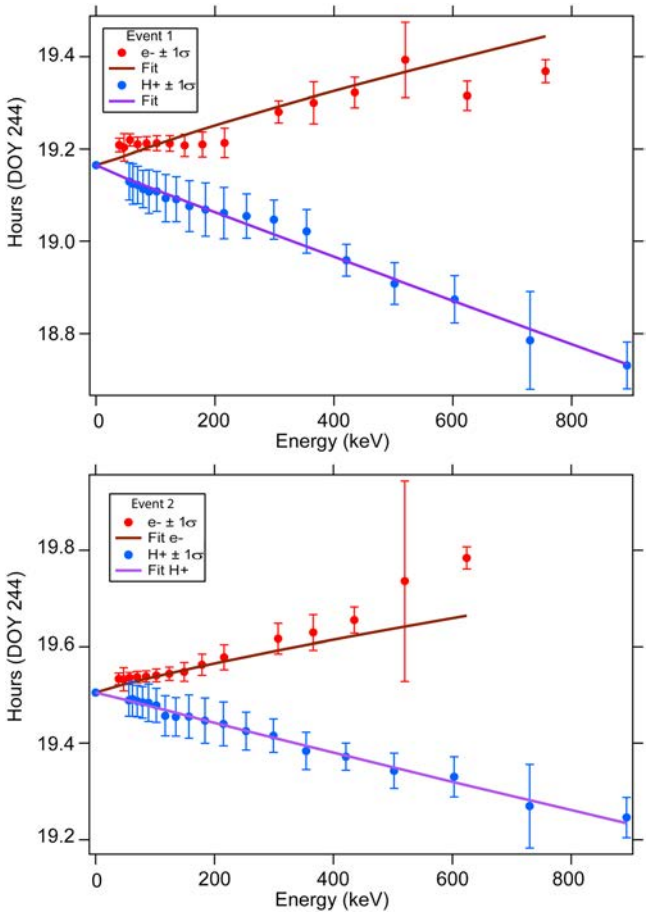

Figure 3. Modeling fitting (solid lines) of two correlated proton (blue symbols) and electron (red symbols) injection event observations. The two events were selected from those in Figures 2a and 2b (see the labels 1 and 2 there). The error bars are one standard deviations of the Gaussian fits, which are larger than the modeled uncertainty in the mean position of the Gaussian.

The lowest energy electrons (below ~200 keV) appear to take on a completely different functional form, looking nearly energy independent. This effect produces an apparent time shift where the electrons appear to be injected sometime after the proton injection. The fits do provide a rough estimate of the age of the injections. They are 11 hr for Event 1 (upper plot) and 7 hr for Event 2 (lower plot). As discussed in section 4.2, these ages may have a role in explaining why these injections are not accompanied by clear auroral signatures.

4. Discussion and Conclusions

4.1. Summary and Novelty of These Observations

We report here new features of dynamic injections at Jupiter not been previously reported. Previous missions have observed mostly electron injections with only the occasional ion injections (Mauk et al., 1999). In the high-latitude regions observed here, proton injections are as common as electron injections. We presume that proton injections are just less visible near the magnetic equator than are electron injections because of the character of the phase space density gradients. This presumption will be the subject of future studies.

We report here the occurrence of very clear injections that are not seen in the auroral images at the magnetic foot points of the injections. This finding is contrary to expectations based on previous work (Dumont et al., 2014, 2018; Mauk et al., 2002) as discussed in section 4.2. The association between auroral images and in situ observations is more complicated than previously assumed.

In this report we show that the behavior of ions and electrons in injection events is different, an observation not previously observed at Jupiter. We speculate the reasons in section 4.3.

These new observations also show a long-duration arching feature that has never been observed at Jupiter. We suggest that this feature is the long-term consequences of injections based on the similarity of this feature with those at Saturn (Paranicas et al., 2010).

4.2. Correlation Between Auroral and In Situ Injections

The presence of hot electrons within the magnetosphere does not necessarily mean that a substantial number of them precipitate continuously to yield a persistent auroral feature. As discussed in section 3, injections can occur many hours prior to the times of the auroral signature observations. Dumont et al. (2014, 2018) concluded, based on Hubble Space Telescope observations, that auroral injection signatures generally have lifetimes of between 0.5 and 1.0 Jupiter rotations (5–10 hr) with some exceptional events lasting somewhat longer (Bonfond et al., 2012). The lifetimes derived by Dumont et al. (2018) were based on a model that assumes that the auroral signature lifetime corresponds to a lifetime of the electron populations themselves. However, it takes little away from that modeling to rather assume that the characteristic time derived is the time for the electrons to stabilize against precipitation rather than the time for that population to be substantially lost. The good correspondence between an in situ and auroral signature reported by Mauk et al. (2002) was for an injection that was 12 hr old, but it is possible that a (much dimmer) nearly dispersionless, and therefore younger, injection occurring at about the same time was responsible for that auroral signature. For the cases reported here, regions of the specific injections measured in situ may have achieved some level of stability with regard to the (presumed) wave-particle scattering (e.g., Bolton et al., 1997; Tao et al., 2010) that is needed to continually move electrons from their stably trapped pitch angles into the pitch angles that precipitate. We note that for most of the events in question here, JEDI does not resolve the loss cone and so cannot be used to estimate precipitating fluxes (see Figure S2).

4.3. Relationship Between Electron and Ion Injections

The dispersion model used to examine the injection timing of these events (Appendix A) fits the shape of the dispersion observed for protons, but it is less successful in fitting the shapes of the electron dispersions. And specifically, the onset of the electron injections (seen first in the lowest energies) is delayed from where it is expected based on the observation of the lower energy protons. We speculate, but do not know for sure, that electrons have more difficulty leaving the region of the injection longitude, perhaps due to gyro-radii effects.

It is likely, and sometime observed for very fresh (undispersed) injections, that there is a magnetic gradient or discontinuity across the boundary between injection plasmas and the surrounding plasmas (Andre et al., 2007; Kivelson et al., 1997; Thorne et al., 1997). The particles must get across that boundary in order to disperse into the broader magnetospheric regions. We speculate that particles with different gyro-radii may have lesser or greater difficulty getting across that boundary. The problem may be similar to the problem of energetic particle escape across a magnetopause. There it is known that the gyro-radii have profound effects (Mauk et al., 2019). Depending on the size of the gyro-radii, particles may spend a substantial amount of time being transported along the boundary (in the radial direction in the case of injections). We would expect that, over time, the magnetic gradients will lessen as the particle disperse. Particles may be initially trapped within the injection region but then released at a later time. All of these speculations will be the subject of deeper analyses in future studies.

Appendix A.: Injection Dispersion Analysis

We describe here a simple quantitative technique for estimating the initial positions and times of the injections (Mauk et al., 1999; Mauk et al., 2005). We assume particles are quickly injected planetward at a specific longitude position, with a broad pitch angle distribution, such that the fresh-injected particles represent a radially extended slab occupying a specific meridian plane. "Quickly" means that the injection process occurs substantially more quickly than the time it takes the particles to significantly disperse in an energy-dependent fashion. Once injected, particles drift around in azimuth by the combined effects of magnetic gradient, magnetic curvature, and rotational electric field drifts. We assume for the inner magnetosphere (<15 R_J) that the azimuthal rate of angular motion from rotational electric field drifts (Ω = Vø/R where Vø is azimuthal speed) is approximately constant with L based on both model and observations (Hill, 1979; McNutt et al., 1981). Magnetic gradient and curvature drifts cause the ions to drift somewhat faster or slower around the planet depending on species.

Within a coordinate system centered on Jupiter but rotationally fixed to the stars, Juno remains roughly within a fixed azimuth plane as it approaches Jupiter. The absolute time T for the spacecraft to encounter a charge particle with a particular energy E and charge Q is given as

$$T = \frac{\Delta\Phi}{\Omega_0 + \Omega_g} + T_0. \tag{1}$$

Note that because the azimuthal motion of the spacecraft is roughly zero, it does not contribute as it does for other missions. Here, $\Delta\Phi$ is the distance in azimuth (radians) travel by the particles from the injection site to the spacecraft, Ω_0 is the rotational electric field drift (+1.745 × 10-4 rad/s for rigid corotation), Ω_g is the combined gradient and curvature drift, and T_0 is the absolute time between injection and observation. For a dipolar configuration, the relativistic Ω_g expression (Hamlin et al., 1961; Lew, 1961), is

$$\Omega_g = 1.384\times10^{-6}\cdot\frac{|e|}{Q}\cdot E(MeV)\cdot\frac{\left(\frac{E(MeV)}{2}+m_0c^2\right)}{(E(MeV)+m_0c^2)}\cdot L\cdot H(\alpha). \tag{2}$$

Here Q is the charge, e is the unit charge, m_0 is the rest mass, and c is the light speed. L is estimated here with the dipole R/Cos2[λm] where R is radial position and λm is magnetic latitude. $H(\alpha)$ is the pitch angle dependence factor. $H(\alpha)$ is estimated with 0.7 + 0.3·Sin(α) as per Hamlin et al. (1961), where α is the equatorial pitch angle. For locally mirroring particles measured at λm, the equatorial pitch angle of that particle, based on first adiabatic invariant conservation, is Sin(α) = (Beq/Bloc)0.5 where, in a dipolar field, Bloc/Beq = (1 + 2·Tan[λm])/Cos5[λm]. Here, "loc" and "eq" local and equatorial.

As the Juno spacecraft travels towards Jupiter and encounters a dispersed injection, we create columns of numbers that comprise: (a) particle energy, (b) absolute arrival times when that energy peaks, (c) L shell position at that time, and (d) magnetic latitude at that time. For the specified values of energy, L, and λm in each row, we simultaneously fit all of the arrival times using equations (1) and (2) by optimizing $\Delta\Phi$ and T_0. We can fit ions alone, electrons alone, or use single optimizations to fit simultaneously the correlated electron and ion injections with a single set of $\Delta\Phi$ and T_0.

Acknowledgments
We are grateful to NASA and contributing institutions that played key roles in making the Juno mission possible. This work was funded by NASA's New Frontiers Program for Juno via subcontract with the Southwest Research Institute in San Antonio. We thank Jack Connerney for input on magnetic mapping, trajectory "wiggle" plots, and reviewing this manuscript. The data used here from the Juno mission are archived and made publicly available from the Planetary Plasma Interactions Node of NASA's Planetary Data System (https://pdsppi.igpp.ucla.edu/).

References

Andre, N., Persoon, A. M., Goldstein, J., Burch, J. L., Louarn, P., Lewis, G. R., et al. (2007). Magnetic signatures of plasma-depleted flux tubes in the Saturnian inner magnetosphere. *Geophysical Research Letters*, *34*, L14108. https://doi.org/10.1029/2007GL030374

Bolton, S. J., Lunine, J., Stevenson, D., Connerney, J. E. P., Levin, S., Owen, T. C., et al. (2017). The Juno Mission. *Space Science Reviews*, *213*(1–4), 5–37. https://doi.org/10.1007/s11214-017-0429-6

Bolton, S. J., Thorne, R. M., Gurnett, D. A., Kurth, W. S., & Williams, D. J. (1997). Enhanced whistler-mode emissions: Signatures of interchange motion in the Io torus. *Geophysical Research Letters*, *24*(17), 2123–2126. https://doi.org/10.1029/97GL02020

Bonfond, B., Gladstone, G. R., Grodent, D., Greathouse, T. K., Versteeg, M. H., Hue, V., et al. (2017). Morphology of the UV aurorae Jupiter during Juno's first perijove observations. *Geophysical Research Letters*, *44*, 4463–4471. https://doi.org/10.1002/2017GL073114

Bonfond, B., Grodent, D., Gérard, J. C., Stallard, T., Clarke, J. T., Yoneda, M., et al. (2012). Auroral evidence of Io's control over the magnetosphere of Jupiter. *Geophysical Research Letters*, *39*, L01105. https://doi.org/10.1029/2011GL050253

Burch, J. L., Goldstein, J., Hill, T. W., Young, D. T., Crary, F. J., Coates, A. J., et al. (2005). Properties of local plasma injections in Saturn's magnetosphere. *Geophysical Research Letters*, *32*, L14S02. https://doi.org/10.1029/2005GL022611

Connerney, J. E. P., Acuña, M. H., & Ness, N. F. (1981). Modeling the Jovian current sheet and inner magnetosphere. *Journal of Geophysical Research*, *86*(A10), 8370–8384. https://doi.org/10.1029/JA086iA10p08370

Connerney, J. E. P., Acuña, M. H., Ness, N. F., & Satoh, T. (1998). New models of Jupiter's magnetic field constrained by the Io Flux Tube footprint. *Journal of Geophysical Research*, *103*(A6), 11,929–11,939. https://doi.org/10.1029/97JA03726

Connerney, J. E. P., Benn, M., Bjarno, J. B., Denver, T., Espley, J., Jorgensen, J. L., et al. (2017). The Juno magnetic field investigation. *Space Science Reviews*, *213*(1-4), 39–138. https://doi.org/10.1007/s11214-017-0334-z

Connerney, J. E. P., Kotsiaros, S., Oliversen, R. J., Espley, J. R., Joergensen, J. L., Joergensen, P. S., et al. (2018). A new model of Jupiter's magnetic field from Juno's first nine orbits. *Geophysical Research Letters*, *45*, 2590–2596. https://doi.org/10.1002/2018GL077312

Dumont, M., Grodent, D., Radioti, A., Bonfond, B., & Gérard, J.-C. (2014). Jupiter's equatorward auroral features: Possible signatures of magnetospheric injections. *Journal of Geophysical Research: Space Physics*, *119*, 10,068–10,077. https://doi.org/10.1002/2014JA020527

Dumont, M., Grodent, D., Radioti, A., Bonfond, B., Roussos, E., & Paranicas, C. (2018). Evolution of the auroral signatures of Jupiter's magnetospheric injections. *Journal of Geophysical Research: Space Physics*, *123*, 8489–8501. https://doi.org/10.1029/2018JA025708

Gérard, J.-C., Bonfond, B., Grodent, D., Radioti, A., Clarke, J. T., Gladstone, G. R., et al. (2014). Mapping the electron energy in Jupiter's aurora: Hubble spectral observations. *Journal of Geophysical Research: Space Physics*, *119*, 9072–9088. https://doi.org/10.1002/2014JA0205

Gladstone, G. R., Persyn, S. C., Eterno, J. S., Walther, B. C., Slater, D. C., Davis, M. W., et al. (2017). The ultraviolet spectrograph on NASA's Juno mission. *Space Science Reviews*, *213*(1-4), 447–473. https://doi.org/10.1007/s11214-014-0040-z

Hamlin, D. A., Karplus, R., Vik, R. C., & Watson, K. M. (1961). Mirror and azimuthal drift frequencies for geomagnetically trapped particles. *Journal of Geophysical Research*, *66*(1), 1–4. https://doi.org/10.1029/JZ066i001p00001

Hill, T. (1979). Inertial limit on corotation. *Journal of Geophysical Research*, *84*(A11), 6554–6558. https://doi.org/10.1029/JA084iA11p06554

Kivelson, M. G., Khurana, K. K., Russell, C. T., & Walker, R. J. (1997). Intermittent short-duration plasma-field anomalies in the Io plasma torus: Evidence for interchange in the Io plasma torus. *Geophysical Research Letters*, *24*(17), 2127–2130. https://doi.org/10.1029/97GL02202

Lew, J. S. (1961). Drift rate in a dipole field. *Journal of Geophysical Research*, *66*(9), 2681–2685. https://doi.org/10.1029/JZ066i009p02681

Mauk, B. H., Clarke, J. T., Grodent, D., Waite, J. H., Paranicas, C. P., & Williams, D. J. (2002). Transient aurora on Jupiter from injections of magnetospheric electrons. *Nature*, *415*(6875), 1003–1005. https://doi.org/10.1038/4151003a

Mauk, B. H., Cohen, I. J., Haggerty, D. K., Hospodarsky, G. B., Connerney, J. E. P., Anderson, B. J., et al. (2019). Investigation of mass/charge-dependent escape of energetic ions across the magnetopauses of Earth and Jupiter. *Journal of Geophysical Research: Space Physics*, *124*. https://doi.org/10.1029/2019JA026626

Mauk, B. H., Haggerty, D. K., Jaskulek, S. E., Schlemm, C. E., Brown, L. E., Cooper, S. A., et al. (2013). The Jupiter Energetic Particle Detector Instrument (JEDI) Investigation for the Juno Mission. *Space Science Reviews*, *213*(1–4), 289–346. https://doi.org/10.1007/s11214-013-0025-3

Mauk, B. H., Saur, J., Mitchell, D. G., Roelof, E. C., Brandt, P. C., Armstrong, T. P., et al. (2005). Energetic particle injections in Saturn's magnetosphere. *Geophysical Research Letters*, *32*, L14S05. https://doi.org/10.1029/2005GL022485

Mauk, B. H., Williams, D. J., McEntire, R. W., Khurana, K. K., & Roederer, J. G. (1999). Storm-like dynamics of Jupiter's inner and middle magnetosphere. *Journal of Geophysical Research*, *104*(A10), 22,759–22,778. https://doi.org/10.1029/1999JA900097

McNutt, R. L., Belcher, J. W., & Bridge, H. S. (1981). Positive ion observations in the middle magnetosphere of Jupiter. *Journal of Geophysical Research*, *86*(A10), 8319–8342. https://doi.org/10.1029/JA086iA10p08319

Paranicas, C., Mitchell, D. G., Roussos, E., Kollmann, P., Krupp, N., Müller, A. L., et al. (2010). Transport of energetic electrons into Saturn's inner magnetosphere. *Journal of Geophysical Research*, *115*, A09214. https://doi.org/10.1029/2010JA015853

Paranicas, C. P., Cheng, A. F., Mauk, B. H., Krimigis, S. M., & Armstrong, T. P. (1990). Ion phase space densities in the Jovian magnetosphere. *Journal of Geophysical Research*, *95*(A12), 20,833–20,838. https://doi.org/10.1029/JA095iA12p20833

Smyth, W. H., & Marconi, M. L. (2006). Europa's atmosphere, gas tori, and magnetospheric implications. *Icarus*, *181*(2), 510–526. https://doi.org/10.1016/j.icarus.2005.10.019

Tao, X., Thorne, R. M., Horne, R. B., Grimald, S., Arridge, C. S., Hospodarsky, G. B., et al. (2010). Excitation of electron cyclotron harmonic waves in the inner Saturn magnetosphere within local plasma injections. *Journal of Geophysical Research*, *115*, A12204. https://doi.org/10.1029/2010JA015598

Thorne, R. M., Armstrong, T. P., Stone, S., Williams, D. J., McEntire, R. W., Bolton, S. J., et al. (1997). Galileo evidence for rapid interchange transport in the Io torus. *Journal of Geophysical Research*, *24*(17), 2131–2134. https://doi.org/10.1029/97GL01788

References From the Supporting Information

Mauk, B. H., Haggerty, D. K., Paranicas, C., Clark, G., Kollmann, P., Rymer, A. M., et al. (2017). Discrete and broadband electron acceleration in Jupiter's powerful aurora. *Nature*, *549*(7670), 66–69. https://doi.org/10.1038/nature23648

Mauk, B. H., Haggerty, D. K., Paranicas, C., Clark, G., Kollmann, P., Rymer, A. M., et al. (2018). Diverse electron and ion acceleration characteristics observed over Jupiter's main Aurora. *Geophysical Research Letters*, *45*, 1277–1285. https://doi.org/10.1002/2017GL076901